J. Fluid Mech. (2005), *vol.* 527, *pp.* 67–84.
DOI: 10.1017/S0022112004002952 Printed in the United Kingdom

The H-trough: a model for liquid metal electric current limiters

By ANDRÉ THESS[1]†, YURII KOLESNIKOV[1], THOMAS BOECK[2], PETER TERHOEVEN[3] AND ANDREAS KRÄTZSCHMAR[3]

[1]Department of Mechanical Engineering, Ilmenau University of Technology, P. O. Box 100565, 98684 Ilmenau, Germany

[2]Laboratoire de Modélisation en Mécanique, Université Pierre et Marie Curie, 4 place Jussieu, Case 162, 75252 Paris Cedex 05, France

[3]Moeller GmbH, Hein-Moeller-Straße 7-11, 53115 Bonn, Germany

(Received 15 January 2004 and in revised form 30 September 2004)

We formulate a simple model which describes the interplay between electromagnetic forces, inertia, and gravity in liquid-metal current-limiting devices utilizing the electromagnetic pinch effect. The dynamics of this system, called an H-trough, is completely described by a nonlinear ordinary differential equation for the fluid's cross-section as a function of time. A bifurcation analysis of stationary states is performed. For a wide range of geometry parameters the cross-section of the fluid is found to be a discontinuous function of the electrical current. The jump in cross-section above some critical current is accompanied by a strong increase of the total electric resistance of the system and results in the current-limiting action of the device by the pinch effect. An experimental study of the system confirms the predicted switching behaviour. For low electric current the experiment is in excellent quantitative agreement with the theory, while for high electric current three-dimensional instabilities and end effects render the agreement with the one-dimensional model less satisfactory. Our model enables us to isolate the pertinent non-dimensional parameters for liquid-metal current limiters and to derive the scaling law of the critical electric current as a function of the geometry and material properties of the system.

1. Introduction and phenomenology

When an electric current passes through an electrically conducting fluid, the interaction of the current with its own magnetic field produces a Lorentz force acting inwardly, which can lead to an instability resulting in a reduction of the cross-section of the fluid. This phenomenon, called the pinch effect, was first observed in a liquid metal in Northrup's classical experiment (Northrup 1907) and has since received considerable attention in plasma physics (Biskamp 1993 and references therein) as well as in liquid-metal magnetohydrodynamics (Murty 1960; Bojarevics *et al.* 1988; Moreau 1990; Davidson 2001).

Recently, the liquid-metal pinch effect has found a new application in electrical engineering for current limiting devices in switchgear assemblies (Terhoeven *et al.* 2001; Berger *et al.* 2001; Thess *et al.* 2002). Traditionally, a current limiter (e.g. a

† Author to whom correspondence should be addressed: thess@tu-ilmenau.de

fuse) is a device which interrupts the electric current in a network in the case of a short-circuit. After removal of the cause of the short-circuit the device has to be replaced or mechanically restored which may incur substantial expenditure, especially in industrial applications characterized by high electric power. In contrast, liquid-metal current limiters exploit the pinch effect which reduces the cross-section of the fluid and thereby leads to a drastic increase of the resistance via ignition of an electric arc. To effectively limit the maximum current this process has to be very fast (a few milliseconds). An important advantage of a liquid-metal current limiter is its 'self-healing' property. When the short-circuit fault is removed, the system returns to its initial state without any external action. Such a device will be useful in low-voltage applications at rated currents ranging from several amperes to several kiloamperes. The self-healing properties and fast reaction times are especially advantageous at breaking short-circuits with high electrical power. In spite of considerable progress in the design of such devices, the understanding of the underlying magnetohydrodynamic (MHD) phenomena is still far from complete. More specifically, no systematic theory is available to date that is capable of describing the dependence of the critical electric current and of the response time on the geometry and other parameters of the system. Although full-scale numerical simulations of the coupled fluid-dynamic–electromagnetic problem for realistic complex geometries provide useful insight, they fail to uncover the basic scaling laws of the system.

The purpose of the present work is to introduce a model for the current-limiting action of the pinch effect in which the mathematical complexity of the governing three-dimensional time-dependent MHD-equations can be reduced to the greatest possible extent, while retaining the intricate interplay among electromagnetic, inertial and gravity forces. After the definition of our system and a qualitative discussion of its steady-state behaviour, we will formulate in § 2 the mathematical model for the general time-dependent case. In § 3 we report results of a numerical bifurcation analysis supplemented by an analytical treatment of the system in the vicinity of its critical point. In § 4 we describe a simple experiment in which we verify the predictions of our model. Section 5 summarizes our conclusions and translates our findings into general scaling relations valid for a broad class of wall-bounded pinch effects under the influence of gravity forces.

Consider the system shown in figure 1 which we shall call the 'H-trough'. Two pairs of vertical plates with a thin gap d are filled with a liquid metal and connected to each other through a thin horizontal slit. By design an electrical current I flows through the left-hand vertical gap only. Then the induced magnetic field gives rise to a Lorentz force which compresses the left-hand fluid column. As a result, the fluid level h decreases and approaches its minimum possible value $h = \ell$ as $I \to \infty$. However, the apparent simplicity of the system is deceptive. Indeed, the system is capable of non-monotonic behaviour including hysteresis.

In order to develop a preliminary understanding of the behaviour of the H-trough we shall briefly discuss its steady states. In a steady state the pressures in the left- and right-hand columns at the location of the horizontal section $z = \ell$ must be equal. The pressure distribution $p(z)$ in the left-hand section, which is the sum of hydrostatic pressure (linear in z) and magnetic pressure (nonlinear in z), is shown in figure 2. For weak electric currents, the hydrostatic pressure dominates, and the curve $z(p)$ is single valued. For strong electric currents, however, the total pressure develops a maximum p_{max} at $z_{max} \approx h/2$, and the function $z(p)$ becomes multiple valued. This property of the pressure distribution turns out to be the key to the switching effect, as will be detailed in § 3.

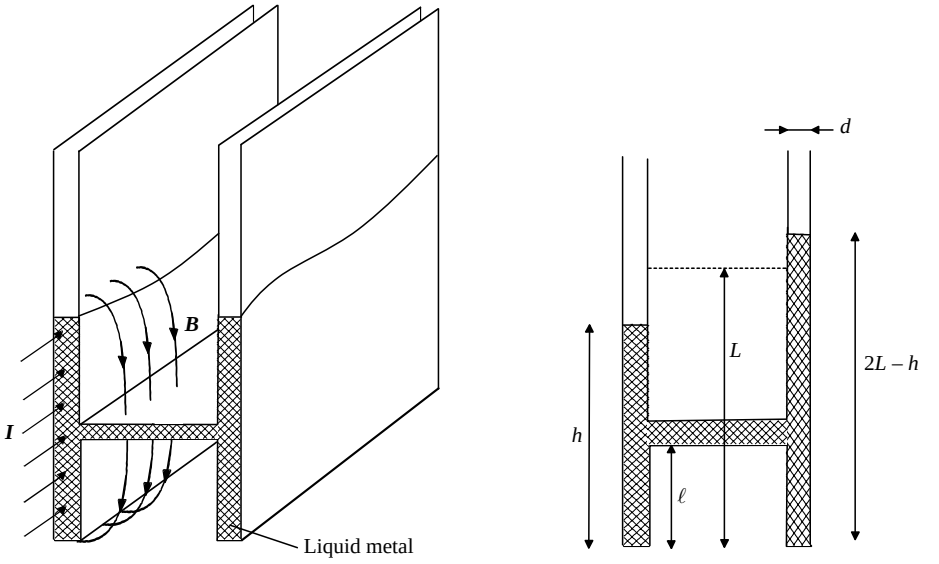

FIGURE 1. Sketch of the system considered. The mass of the fluid in the horizontal section is assumed to be negligibly small. The origin of the x-axis is at the bottom of the left-hand vertical section.

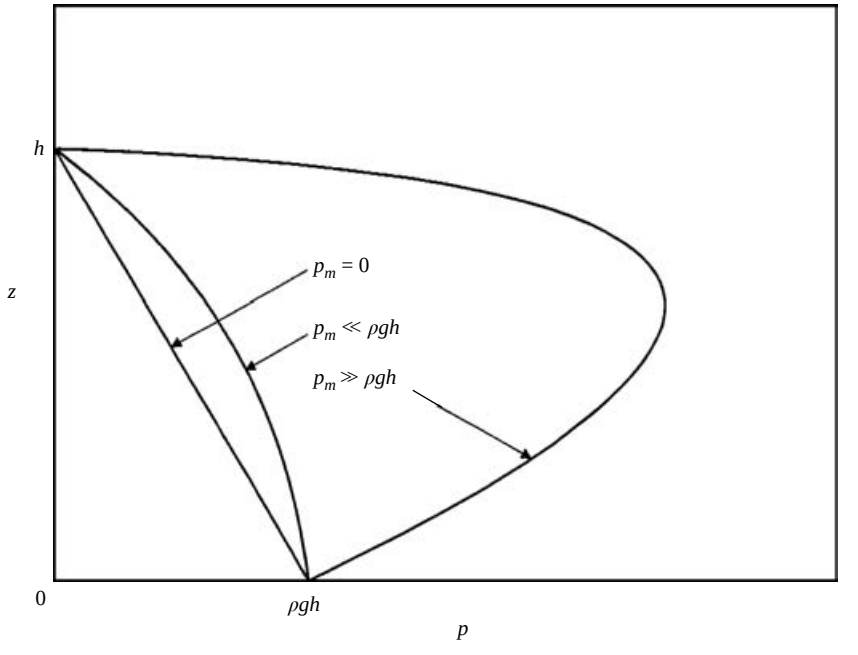

FIGURE 2. Schematic of the pressure distribution in the left-hand column of the H-trough.

The family of steady states $h(I, L, \ell)$ whose exact shape will emerge in § 3 as one of the numerical results, is shown in figure 3. For low filling levels, i.e. $L < L_c$ the fluid height turns out to be a monotonically decreasing function of the electric current. When L exceeds a critical value L_c the dependence of h on I ceases to be monotonic. Upon exceeding a certain threshold of the current, h jumps to a much lower value. This jump is accompanied by a drastic decrease of the fluid's cross-section and an

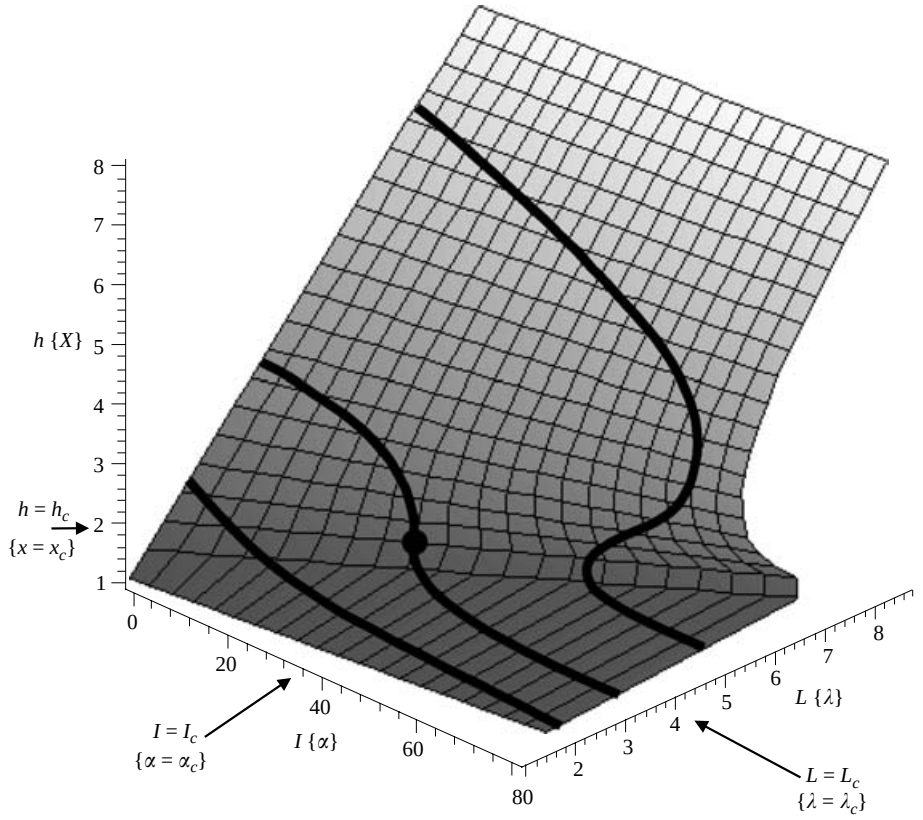

FIGURE 3. Qualitative behaviour of steady states of the H-trough. The bracketed symbols are non-dimensional quantities introduced in § 2. (L_c, I_c, h_c) is referred to as the critical point.

increase of the resistance. When the current is reduced, the system jumps back to its initial state after some hysteresis.

The remainder of the paper is devoted to a theoretical and experimental determination of the steady states of the H-trough and their stability. We parenthetically note that the H-trough represents one of the rare examples of MHD problems which are amenable to rigorous analytic treatment. Moreover, the H-trough may serve as an illustrative example "for those engaged in research to learn from the interesting practical problems in industrial fluid mechanics" (Hunt 1991, p. 3) in general, and in MHD (Davidson 1999) in particular.

2. Formulation of the mathematical model

We use Cartesian coordinates (x, y, z) with x measuring the distance from the left-hand liquid column, y being parallel to the electric current, and z pointing upward, whereby the bottom of the trough is located at $z = 0$. The mathematical model for the H-trough is based on the assumptions (i) that the liquid metal is an inviscid incompressible fluid, (ii) that the width of the gap d is very small (i.e. $d \ll h$), (iii) that the electric current density of our infinitely long system is independent of z, and (iv) that the free surface of the fluid does not support surface waves (i.e. h is independent of y). The second and third assumptions allow us to use the current and magnetic field distribution in a thin sheet to compute the Lorentz force in the liquid.

Assumption (iv) is made in order to describe the flow by a single variable, namely the time-dependent height $h(t)$ of the liquid metal in the left-hand column.

The governing equations for $h(t)$ can be derived in a rigorous way by expressing the kinetic, potential, and magnetic energy of the system in terms of h and $\mathrm{d}h/\mathrm{d}t$, by constructing the Lagrange function, and deriving the equation of motion by following the standard procedure known from classical mechanics. However, we find it more appropriate to present an intuitive formulation here, since this gives a better insight into the physics of the problem.

In order to derive the equation of motion we need to determine the hydrostatic pressure distributions $p_R(z)$ and $p_L(z)$ in the right- and left-hand column, respectively. The Lorentz force in the left-hand column generates an additional magnetic pressure besides the usual hydrostatic pressure due to gravity. To compute the magnetic field we need to know the electric current density $\boldsymbol{J}$. In a real system with finite length in y, this quantity would have to be determined by solving a Laplace equation $\nabla^2\Phi = 0$ for the electric potential Φ from which the electric current density could be computed as $\boldsymbol{J} = -\sigma\nabla\Phi$. Since we have assumed that our system is unbounded in y, and that the thickness of the left-hand column is independent of z, we can prescribe the electric current density as

$$\boldsymbol{J}(x, z) = \frac{I}{h}\,\delta_d(x)[\Theta(z) - \Theta(z-h)]\boldsymbol{e}_y. \tag{2.1}$$

In this expression, I/h represents a constant line density of the total current I, Θ is the Heaviside step function, and $\delta_d(x)$ is defined as $\delta_d = 1/d$ for $|x| \leqslant d/2$ and $\delta_d = 0$ for $|x| > d/2$. We only need to compute the horizontal component of the (two-dimensional) magnetic field at the position of the current sheet. This is most easily accomplished by introducing a magnetic potential $\psi(x, z)$ via $B_x = \partial\psi/\partial z$ and $B_z = -\partial\psi/\partial x$, which automatically satisfies the condition $\nabla\cdot\boldsymbol{B} = 0$. Ampere's equation $\mu_0\boldsymbol{J} = \nabla\times\boldsymbol{B}$ then becomes

$$\frac{\partial^2\psi}{\partial x^2} + \frac{\partial^2\psi}{\partial z^2} = -\mu_0 J(x, z) \tag{2.2}$$

where $J(x, z) = \boldsymbol{J}\cdot\boldsymbol{e}_y$. For the current distribution (2.1) the solution of (2.2) satisfying the condition $|\nabla\psi| \to 0$ at infinity is

$$\psi(x, z) = -\frac{\mu_0}{2\pi}\int\int J(x', z')\ln|\boldsymbol{r} - \boldsymbol{r}'|\,\mathrm{d}x'\,\mathrm{d}z'. \tag{2.3}$$

This solution can be evaluated explicitly at $x = 0$ if the current sheet is assumed to be infinitely thin, i.e. $d \to 0$. In this case $\delta_d(x)$ becomes a delta function and the integral simplifies to

$$\psi(0, z) = -\frac{\mu_0 I}{2\pi h}\int_{z'=0}^{z'=h}\ln|z - z'|\,\mathrm{d}z' \tag{2.4}$$

The necessary integration can be done analytically. For $0 < z < h$ we obtain the magnetic field as

$$B_x(0, z) = \frac{\mu_0 I}{2\pi h}\ln\left(\frac{z}{h-z}\right). \tag{2.5}$$

Notice that B_x, the normal component of the magnetic field, is not singular in the limit $d \to 0$; so (2.5) can be used for the computation of the Lorentz force as if B_x were independent of x. The vertical component f_z of the Lorentz force density $\boldsymbol{f} = \boldsymbol{J}\times\boldsymbol{B}$ is

$$f_z(x, z) = -\frac{\mu_0 I^2}{2\pi h^2}\delta_d(x)[\Theta(z) - \Theta(z-h)]\ln\left(\frac{z}{h-z}\right). \tag{2.6}$$

Notice that B_x and f_z are odd functions with respect to $z = h/2$. The magnetic pressure gradient satisfies $\mathrm{d}p_m/\mathrm{d}z = f_z$. The integration can again be performed analytically. Taking into account that $\delta_d = 1/d$ in the fluid, the magnetic pressure becomes

$$p_m(z) = -\frac{\mu_0 I^2}{2\pi h^2 d}\left\{ z \ln\left(\frac{z}{h-z}\right) + h \ln\left(\frac{h-z}{h}\right)\right\}. \tag{2.7}$$

The magnetic pressure is positive for $0 < z < h$, symmetric with respect to $z = h/2$ and vanishes at $z = 0$ and $z = h$.

For deriving the equation of motion we shall now stipulate that the left-hand liquid column has height h and the right-hand column $2L - h$ due to the conservation of mass. The hydrostatic pressure in the left-hand column is the sum of the gravitational and the magnetic contributions, i.e.

$$p_L(z) = \rho g(h - z) + p_m(z). \tag{2.8}$$

The behaviour of this pressure is schematically shown in figure 2. In the right-hand column, the hydrostatic pressure is given by

$$p_R(z) = \rho g(2L - h - z). \tag{2.9}$$

To obtain the equation of motion for h, we need to apply Newton's law to each column of liquid above the horizontal channel (located at height $z = \ell$) on either side of the apparatus. The net force acting on each column is the sum of the integrated body force density and the difference of the pressure Π between the bottom and the top of the liquid column. The integrated body force density can be represented by the difference in hydrostatic pressure between top and bottom ($z = \ell$) of the liquid column. For the left-hand column we have (per unit length in y)

$$(h - \ell)\rho d \frac{\mathrm{d}^2}{\mathrm{d}t^2}(h - \ell) = d[\Pi_L(\ell) - \Pi_L(h) + p_L(h) - p_L(\ell)], \tag{2.10}$$

where Π_L denotes the pressure in the left-hand column. The corresponding equation for the right-hand column is

$$(2L - h - \ell)\rho d \frac{\mathrm{d}^2}{\mathrm{d}t^2}(2L - h - \ell) = d[\Pi_R(\ell) - \Pi_R(2L - h) + p_R(2L - h) - p_R(\ell)]. \tag{2.11}$$

By subtracting these equations we obtain

$$2(L - \ell)\rho d \frac{\mathrm{d}^2 h}{\mathrm{d}t^2} = d[\Pi_L(\ell) - \Pi_L(h) - p_L(\ell) + p_L(h) - \Pi_R(\ell) + \Pi_R(2L - h) + p_R(\ell) - p_R(2L - h)]. \tag{2.12}$$

We can now simplify the right-hand side by observing that the pressure at the top is the ambient pressure, i.e.

$$\Pi_L(h) = \Pi_R(2L - h). \tag{2.13}$$

We shall also neglect the fluid mass in the horizontal channel, whereby the pressure must be the same on either side of the horizontal channel, i.e.

$$\Pi_L(\ell) = \Pi_R(\ell). \tag{2.14}$$

Thus, we obtain the equation of motion

$$2(L - \ell)\rho d \frac{\mathrm{d}^2 h}{\mathrm{d}t^2} = d[p_R(\ell) - p_L(\ell)], \tag{2.15}$$

where we have observed that the hydrostatic pressures are zero at the top surfaces.

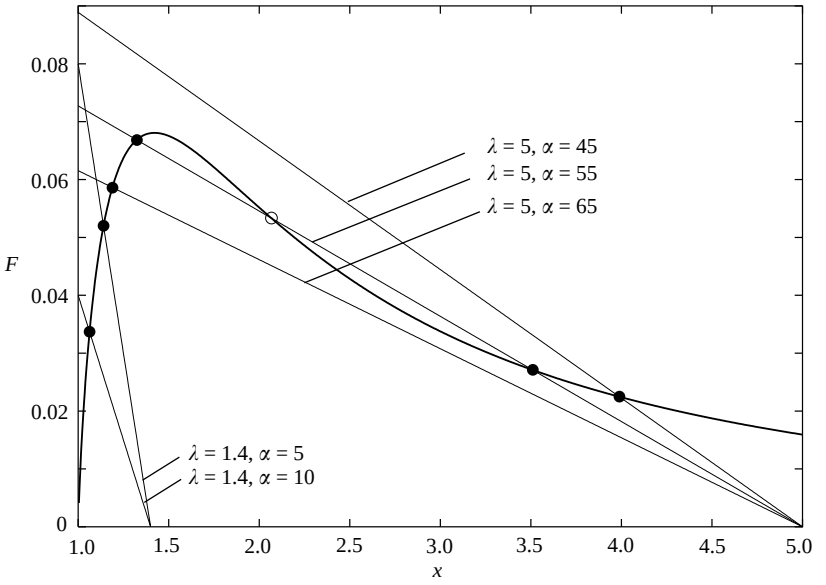

FIGURE 4. Graphical solution of (3.1): Non-dimensional function $F(x)$ defined in (2.18) (full line) together with the function $(\lambda - x)/\alpha$ (thin lines). Filled [open] circles represent stable [unstable] solutions.

The height ℓ is an important parameter in this equation. If the electric current were zero, the liquid would oscillate at a frequency depending only on the length of the U-shaped column above and including the channel. Equation (2.15) with (2.8) and (2.9) is the desired equation of motion for $h(t)$. The same equation would have been obtained by using the Lagrange method, as mentioned earlier.

The mathematical model can be written in a more compact form by introducing non-dimensional fluid level x and time τ according to

$$x = \frac{h}{\ell}, \qquad \tau = \sqrt{\frac{g}{L-\ell}}\,t. \tag{2.16}$$

Our new dynamical variable x should not be confused with the coordinate across the gap, defined in figure 1. The differential equation for $x(\tau)$ then becomes

$$\frac{\mathrm{d}^2x}{\mathrm{d}\tau^2} + x = \lambda - \alpha F(x), \tag{2.17}$$

where

$$F(x) = -\frac{1}{2\pi x}\left\{ \ln\left(\frac{x-1}{x}\right) - \frac{1}{x}\ln(x-1)\right\} \tag{2.18}$$

is a dimensionless function shown in figure 4, which describes the magnetic pressure. Our equation contains two dimensionless parameters. The forcing parameter

$$\alpha = \frac{\mu_0 I^2}{2\rho g d \ell^2} \tag{2.19}$$

describes the strength of the electromagnetic forces in relation to the gravity force. The filling parameter

$$\lambda = \frac{L}{\ell} \tag{2.20}$$

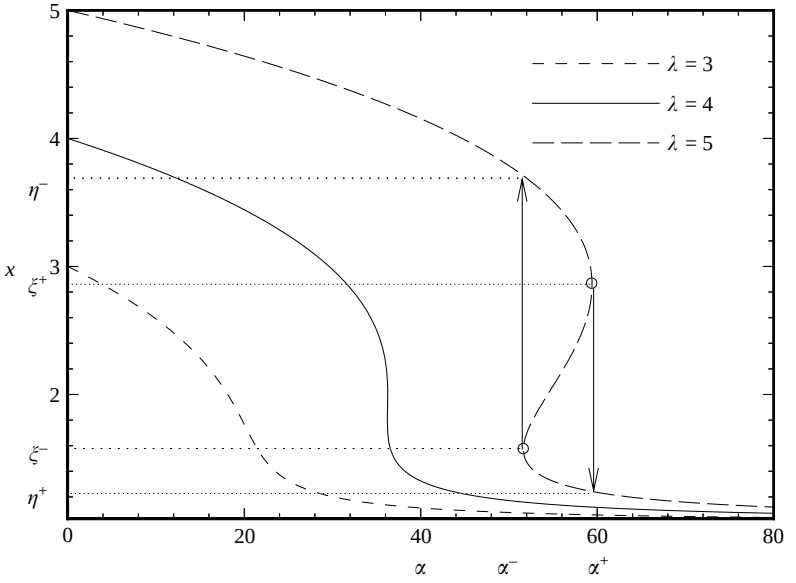

FIGURE 5. Steady solution curves for x depending on α. The limit points of the upper and lower branch for $\lambda = 5$ are marked with circles. The solution changes discontinuously at these points (i.e. it jumps from one branch to the other). The 'jump origins' are denoted by ξ^+, ξ^-, and the corresponding 'jump destinations' by η^+, η^-.

is a non-dimensional measure of the initial filling level. For a prescribed forcing α and a given initial filling λ the nonlinear differential equation (2.17) with (2.18) determines the time-dependence of the fluid level in the H-trough.

3. Analysis of steady states

3.1. *Numerical solution*

In mechanical equilibrium (2.17) simplifies to

$$\lambda - x = \alpha F(x). \tag{3.1}$$

This equation determines the family of steady states $x(\lambda, \alpha)$ shown in figure 3 whereby $x > 1$. Remember that x is the non-dimensional filling level, α the electromagnetic forcing parameter and λ the initial filling level. The general behaviour of the steady solutions can be best understood by a graphical solution of (3.1) with reference to figure 4. Observe that the solution of (3.1) is the intersection between the magnetic pressure function $F(x)$ and the function $(\lambda - x)/\alpha$, both shown in figure 4. $F(x)$ rises monotonically from $F = 0$ at $x = 1$ to a maximum at $x_m \approx 1.4215$ and tends to zero as $x \to \infty$. As long as $\lambda < x_m$ the intersection is located on the monotonically increasing branch of $F(x)$, and there can only be one solution x for any $\alpha > 0$. For $\lambda > x_m$ it becomes possible that there are three solutions for certain values of α.

We analyse the algebraic bifurcation problem (3.1) numerically using the software package AUTO97 for continuation and bifurcation analysis (Doedel 1981; Doedel *et al.* 1998). In a first step, we prescribe λ and compute $x(\lambda, \alpha)$ by continuation in the parameter α. The starting point is the trivial solution $x = \lambda$ for $\alpha = 0$ ($I \equiv 0$). Figure 5 shows results for several values of λ.

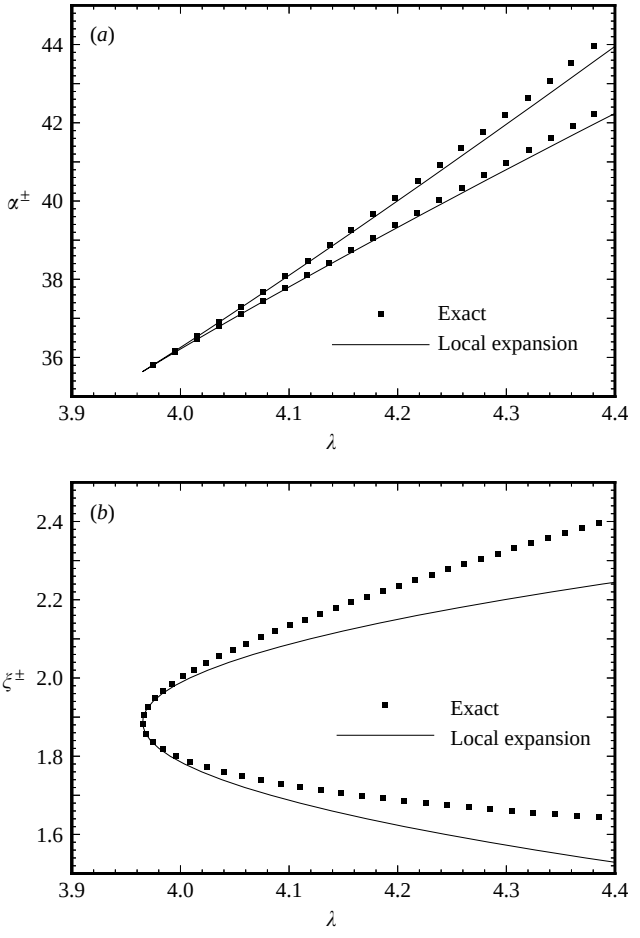

FIGURE 6. Bifurcation curves near the critical point. (*a*) Bifurcation set (cusp) given by the curves $\alpha^{+}(\lambda)$ and $\alpha^{-}(\lambda)$ together with the local expansion (3.18). (*b*) Location of the 'jump origins' ξ^{+}, ξ^{-}, together with the local expansion (3.15).

For $\lambda = 3$ there is only one solution x for any $\alpha > 0$. This behaviour changes at larger values of λ, in agreement with our foregoing discussion. For $\lambda > \lambda_c$, which is represented in figure 5 by the curves for $\lambda = 4$ and $\lambda = 5$, there exists an interval (α^{-}, α^{+}) with three roots for x. The end points of this interval are the limit (bifurcation) points of the upper solution branch [denoted by (α^{+}, ξ^{+})] and the lower solution branch [denoted by (α^{-}, ξ^{-})], which are connected by a third branch. We will later see that this third branch is unstable.

The observed behaviour is typical of a scalar equation with two parameters (Seydel 1994). The solution manifold is of the cusp type, which is named after the form of the region in parameter space (λ, α) where three solutions coexist (figure 6*a*). The next step in the bifurcation analysis is to compute the boundaries of the cusp,† i.e. we have to trace the limit points as functions of λ. The AUTO97 software also allows us to perform this computation. Figure 6 shows the functions $\alpha^{\pm}(\lambda)$ and $\xi^{\pm}(\lambda)$, which

† The cusp boundary is the bifurcation set, i.e. the parameter values (λ, α), for which the solution changes qualitatively.

we call 'jump origins'. They merge at the critical point

$$\lambda_c \approx 3.965, \qquad x_c \approx 1.8867, \qquad \alpha_c \approx 35.637. \tag{3.2}$$

From a practical viewpoint it is not only important to know where the solution changes discontinuously, but also by how much. We have therefore not only computed the limit points $\xi^{\pm}(\lambda)$, but also the corresponding values $\eta^{\pm}(\lambda)$ on the continuous branches, which we call 'jump destinations' (see figure 5). Together with the 'jump origins' $\xi^{\pm}$, they determine the discontinuous jump from one branch to the other and thus the change of resistivity of the device.

The transition from monotonic to non-monotonic behaviour can be understood by invoking the spatial distribution of the pressure in the left-hand section, shown in figure 2. Recall that for weak electric currents, the hydrostatic pressure dominates, and the curve $z(p)$ is single valued. For strong electric currents, the total pressure develops a maximum p_{max} at $z_{max} \approx h/2$, and the function $z(p)$ becomes multiple valued. If the pressure maximum is located below the horizontal section, which is the case for low filling levels, an increase of the electric current will compress the left-hand column and displace the pressure maximum further away from $z = \ell$, resulting in a monotonic decrease of $h(I)$. This situation should be contrasted with the case when the pressure maximum is above $z = \ell$. Here the joint action of pressure rise due to increasing I and of pressure rise due to z_{max} approaching ℓ can no longer be compensated by a higher hydrostatic pressure difference once the current has exceeded some critical value. As a result, the state is no longer stable and the system jumps to another equilibrium with lower h.

When the system jumps from a state with $x \sim \lambda$ to a state with $x \ll \lambda$ it not only changes its electrical resistivity (which is proportional to x^{-1}) but also its mechanical stiffness. This feature is revealed by considering the frequency $\omega_0(\lambda, \alpha)$ of small-amplitude oscillations around a steady state x_0. Considering time-dependent states of the form $x(\tau) = x_0 + \epsilon(\tau)$ and linearizing (2.17) with respect to the infinitesimal perturbation ϵ, it can be readily shown that the frequency of small-amplitude oscillations is given by

$$\omega_0^2 = 1 + \alpha F'(x_0). \tag{3.3}$$

The AUTO97 software can compute this frequency as it traces the stationary solution branch. Figure 7 shows the result for $\lambda = 5$. For $\alpha = 0$ we have $\omega_0 = 1$ (not shown) which corresponds to free oscillations of an ideal fluid in a U-shaped column. When the electric current is switched on, this oscillation frequency decreases monotonically with α and tends to zero as $\alpha \to \alpha^+$ (point A in figure 7). When α is increased beyond α^+, the system jumps to point B. This branch is characterized by a higher frequency of oscillations, indicating that the system is more 'stiff' in the bifurcated state. When α is decreased beyond α^-, the system jumps back from C to D. The branch with $\omega_0^2 < 0$ extending between α^- and α^+ indicates that the third solution is unstable.

3.2. *Asymptotic solution for* $\lambda \to \lambda_c$

Since it is of considerable practical interest to understand the system in the vicinity of the critical point $(\lambda_c, \alpha_c, x_c)$ we shall now analytically investigate the behaviour in this part of the parameter space, which is shown more clearly in figure 6. The bifurcation points $\xi^{\pm}(\lambda)$ and $\alpha^{\pm}(\lambda)$ are determined by

$$\frac{\partial \alpha(\lambda, \xi)}{\partial \xi} = \frac{\partial}{\partial \xi}\left\{ \frac{\lambda - \xi}{F(\xi)} \right\} = 0. \tag{3.4}$$

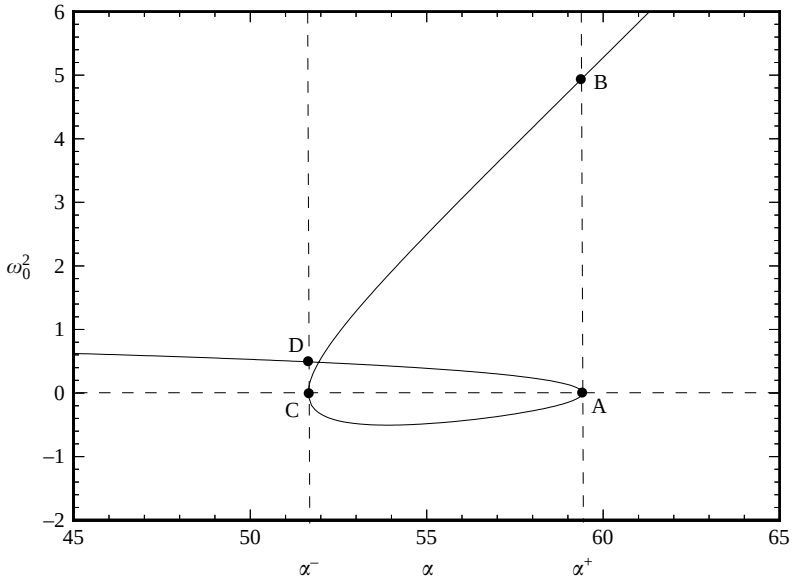

FIGURE 7. Frequency of small-amplitude oscillations about the steady states of the H-trough for $\lambda = 5$. When α is increased beyond α^+, the system jumps from A to B. When α becomes smaller than α^-, the jump is from C to D.

The critical point λ_c is characterized by a double zero because the bifurcation points $\xi^{\pm}(\lambda_c)$ coincide, i.e.

$$\frac{\mathrm{d}^2\alpha(\lambda, \xi)}{\mathrm{d}\xi^2} = 0. \tag{3.5}$$

From this equation and the solutions

$$\lambda - \xi(\lambda) = -F(\xi(\lambda))/F'(\xi(\lambda)), \qquad \alpha(\lambda) = -1/F'(\xi(\lambda)). \tag{3.6}$$

of (3.4) for the bifurcation points we find the critical point condition

$$F''(x_c) = 0. \tag{3.7}$$

The Taylor series of F about $\xi = x_c$ has the form

$$F(x_c + \tilde{\xi}) = A + B\tilde{\xi} + C\tilde{\xi}^3/6 + \ldots, \tag{3.8}$$

where $\xi = x_c + \tilde{\xi}$, $\lambda = \lambda_c + \tilde{\lambda}$, and $\alpha = \alpha_c + \tilde{\alpha}$. The coefficients in this series are $A = (\lambda_c - x_c)/\alpha_c$, $B = -1/\alpha_c$, $C \approx 0.0916$. We now substitute the expansion (3.8) into equations (3.6). This provides one relation between $\tilde{\xi}$ and $\tilde{\lambda}$ and one between $\tilde{\xi}$ and $\tilde{\alpha}$:

$$\tilde{\lambda}(B + C\tilde{\xi}^2/2 + \ldots) = (\tilde{\xi} + A/B)(C\tilde{\xi}^2/2 + \ldots) - (C\tilde{\xi}^3/6 + \ldots), \tag{3.9}$$

$$\tilde{\alpha}(B + C\tilde{\xi}^2/2 + \ldots) = (C\tilde{\xi}^2/2 + \ldots)/B. \tag{3.10}$$

To obtain a non-trivial relation $\tilde{\xi}(\tilde{\lambda})$ we retain terms up to second order. We find

$$\tilde{\xi}^2 = \frac{2B^2}{AC}\,\tilde{\lambda}. \tag{3.11}$$

For $\tilde{\alpha}(\tilde{\lambda})$ we divide (3.9) by (3.10) and retain only linear terms in $\tilde{\xi}$ on the right-hand side. We then solve for $\tilde{\alpha}$ using (3.11) and obtain

$$\tilde{\alpha} = \tilde{\lambda}/A \pm \tilde{\lambda}^{3/2}\frac{2B^2}{3A^2}\left(\frac{2}{AC}\right)^{1/2}. \tag{3.12}$$

Reverting to the original variables α, λ, the desired asymptotic solutions in the vicinity of the critical point are

$$\xi^{\pm} = x_c \pm \left[\frac{2B^2}{AC}(\lambda - \lambda_c)\right]^{1/2}, \tag{3.13}$$

$$\alpha^{\pm} = \alpha_c + \frac{\lambda - \lambda_c}{A} \pm (\lambda - \lambda_c)^{3/2}\frac{2B^2}{3A^2}\left(\frac{2}{AC}\right)^{1/2}. \tag{3.14}$$

Figure 6 shows that the solutions (3.13), (3.14) are in excellent agreement with the exact numerical values close to λ_c.

3.3. *Asymptotic solution for* $\lambda \to \infty$

The limit of large filling levels (where the initial fluid height $h = L$ is far above the height ℓ of the horizontal section) can be analytically investigated by invoking equations (3.6) and the asymptotic behavior of $F^{-1}\mathrm{d}F(x)/\mathrm{d}x$. We shall not present this analysis here. We instead quote the final result for the bifurcation curves in the form

$$\xi^{-} \to x_m \approx 1.4215, \quad \xi^{+} \sim 2\lambda/3, \tag{3.15}$$

and

$$\alpha^{+} \sim \pi(2\lambda/3)^3/\ln(2\lambda/3), \quad \alpha^{-} \sim \lambda/F(x_m) \approx 14.69\lambda. \tag{3.16}$$

These expressions are found to be in excellent agreement with the exact numerical results for large values of λ.

4. Experimental results

We tested our theoretical predictions by building two laboratory models of the H-trough differing by their length L_y and electrode height L_z, shown in the insets of figure 8. The model with $L_y = 14.6\,\mathrm{mm}$ and $L_z = 100\,\mathrm{mm}$ will be referred to as the 'long trough' whereas the model with $L_y = 5.5$ mm and $L_z = 130\,\mathrm{mm}$ is referred to as the 'short trough'. The design of the troughs is almost entirely identical to the sketch in figure 1 and will therefore not be discussed in detail here. Both models are made of Plexiglas. The width of the vertical gaps $d = 1\,\mathrm{mm}$, which is equal to the width of the electrodes, is chosen as small as possible in order to keep the electric heat generation low. The horizontal connection between the two vertical chambers, located at $\ell = 26.4\,\mathrm{mm}$, consists of a thin pipe 4 mm in diameter. The troughs are filled with liquid metal. We use a Ga–In–Sn eutectic alloy with a density $\rho = 6363\,\mathrm{kg\,m^{-3}}$ and an electrical conductivity $\sigma = 3.307 \times 10^6\,\Omega^{-1}\,\mathrm{m}^{-1}$ as the working fluid. Its free surface is covered by an ethanol layer with 2% HCl added in order to prevent oxidation and to improve the wetting properties of the liquid metal. Alternating current (AC) with a fixed frequency of 50 Hz and a variable strength in the range $0 < I < 1500\,\mathrm{A}$ is injected into the liquid metal by two water-cooled copper electrodes. Using AC rather than DC current has the advantage that we can easily measure the magnetic field outside the system by using small induction coils. This independent measurement technique is useful in analysing the dynamical behaviour of our system, which, however, is outside the scope of the present paper. Notice that the frequency of the electric current is still low enough for the skin effect to be negligible.

Each experiment is started by filling the trough to a low level $L \ll L_z$. The electric current is then gradually increased from zero, and the fluid level h is recorded as a function of I as soon as the system has settled at a steady state. This procedure is repeated for increasingly large L until the maximum filling level $L = L_z$ is reached.

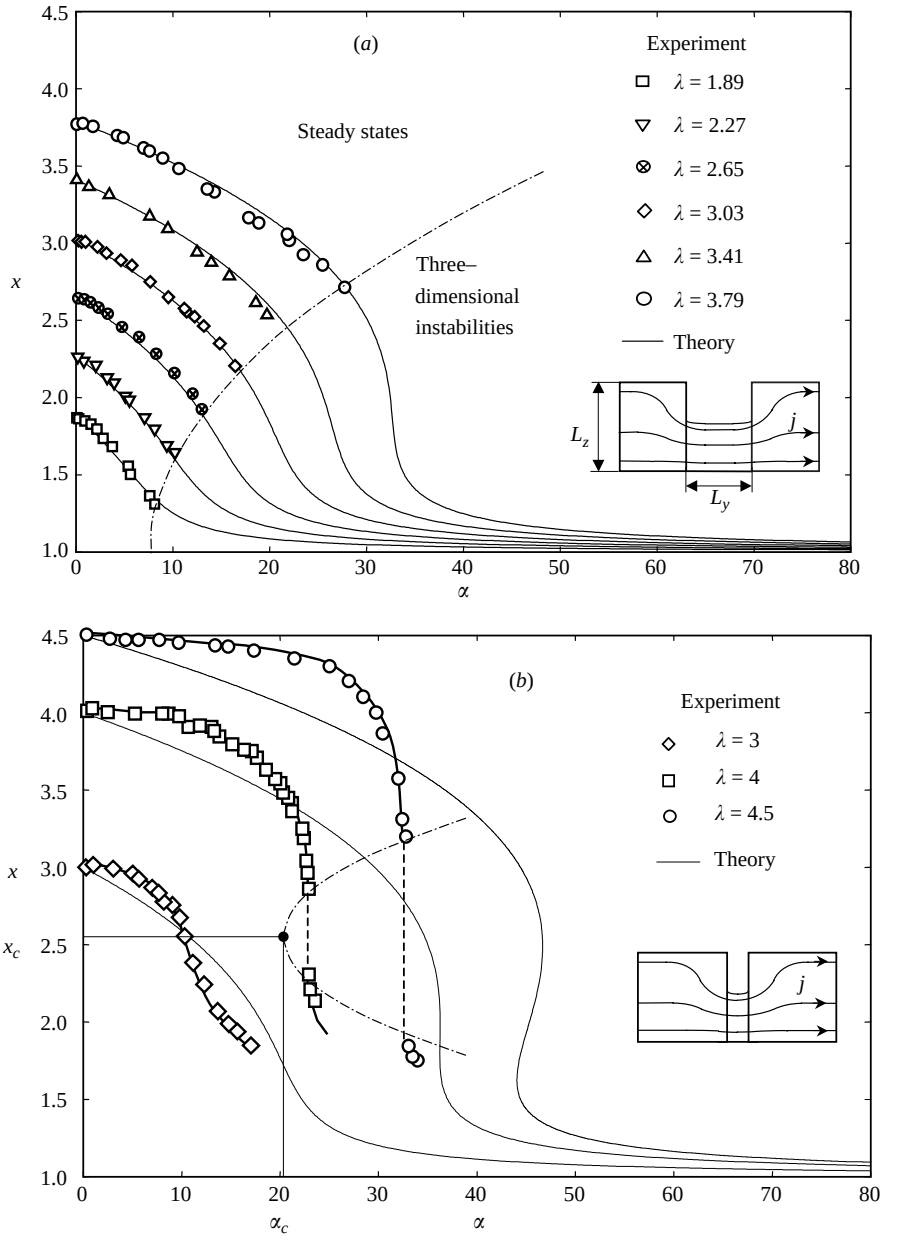

FIGURE 8. Comparison between experimental and theoretical results for the steady states of an H-trough. (*a*) Long trough with $L_y = 14.6\,\text{mm}$ and $L_z = 100\,\text{mm}$, (*b*) short trough with $L_y = 5.5\,\text{mm}$ and $L_z = 130\,\text{mm}$. Insets illustrate the different levels of non-uniformity of the electric current density in the liquid metal.

The results of our experimental investigations, shown in figure 8, can be summarized in just two sentences. The long trough shows an excellent quantitative agreement with the theoretical predictions, but observation of the switching effect is prevented by three-dimensional instabilities. The short trough clearly confirms the existence of the switching effect but agrees with the theory only qualitatively due to its very limited length.

Figure 8(*a*) shows the steady states obtained in the long trough. The agreement with the theoretical predictions is remarkable, given the highly simplified nature of the mathematical model. However, the experimental curves are limited by the onset of instabilities at the free surface of the current-carrying liquid metal which are excluded from our analysis. It was observed that above a critical electric current, roughly given by $\alpha \sim \lambda^2$ (cf. the parabola in figure 8*a*), unstable waves emerged at the surface. If the current was not switched off, nonlinear evolution transformed the wave into a finger, which, upon its rapid touchdown, created arc effects and lead to a violent boiling of the covering liquid. Similar observations were reported in the earlier experiment of Northrup (1907) and are known to occur in various other electrically driven vortical flows (Bojarevics *et al.* 1998).

In order to suppress the three-dimensional instabilities, the short trough was used. The hypothesis that a short trough is less prone to three-dimensional instabilities than a long one rests on the assumption that in the present system long waves are the most 'dangerous' modes. Although we did not perform a stability analysis, we believe that $I_c(k)$, the critical electric current for three-dimensional instabilities as a function of the wavenumber k, is a monotonically increasing function with its minimum at $k = 0$. Such behaviour is supported by recent observations of pinch phenomena in an annular liquid metal sheet under the influence of a high-frequency magnetic field (Mohring, Karcher & Schulze 2004).

Figure 8(*b*) confirms the existence of the predicted switching effect. It is clearly seen that for sufficiently high initial filling level the system jumps to a bifurcated state characterized by low x. Visual observation of the fluid surface in these states shows surface fluctuations with a much higher frequency than in the initial condition, in agreement with the behaviour of small-amplitude oscillations shown in figure 7. Hysteresis was not observed, probably due to the fact that only slightly supercritical values of λ were accessible in our experiment. While in good qualitative accord with theory, the quantitative agreement of the short trough with the predictions, shown with thin solid lines in figure 8, is less satisfactory. The reason for this is twofold. On the one hand, the electric current density in the short trough is far from homogeneous in the y-direction. The electric current lines emanating from the long copper electrodes become compressed when entering the liquid metal, leading to a strong deviation from the assumption underlying our theory. On the other hand, fluid flow within the liquid metal, which is driven by the rotational part of the Lorentz force (not present in our theory), destabilizes the system leading to the observed unstable waves and subsequent nonlinear switching effects. Recent computations of steady states by using (3.1) with a function $F(x)$ obtained from a full three-dimensional finite-element computation of the Lorentz force taking into account the finite length of the system (Gerner 2004) lead to a better, albeit still imperfect, agreement with the experiment. This observation indicates that in order to fully reproduce the behaviour of the experimental systems, a three-dimensional solution of the coupled electromagnetic–fluid dynamic problem is necessary, which is beyond the scope of this paper. In spite of these facts, the experimentally determined critical point

$$\lambda_c = 3.9 \pm 0.3, \quad x_c = 2.6 \pm 0.2, \quad \alpha_c = 21 \pm 4 \tag{4.1}$$

is in reasonable agreement with the theoretical values

$$\lambda_c = 3.965, \quad x_c = 1.8867, \quad \alpha_c = 35.637 \tag{4.2}$$

(cf. (3.2)). The uncertainties are due to an inaccuracy of about 2.5% in the determination of h, electric current fluctuations and measurement uncertainty of about

	Ga–In–Sn		Na–K & Kerosene	
System	$d = 1$ mm	$d = 5$ mm	$d = 1$ mm	$d = 5$ mm
I_c (A)	297	3323	8.34	93.2
U_c (V)	0.476	1.063	0.0179	0.0400
P_c (W)	141	3531	0.149	3.72
R_c (mΩ)	1.60	0.316	2.15	0.430
L_c (mm)	19.8	99.0	19.8	99.0
h_c (mm)	9.45	47.2	9.45	47.2

TABLE 1. Physical parameters for two different fluid systems at the critical point.

2%, and an estimated uncertainty of 2.5% for the thermophysical properties of our working liquid.

5. Summary and discussion

We have formulated a simple mathematical model describing the basic mechanism of liquid-metal current limiters and verified its validity by a series of model experiments.

In order to derive general practical conclusions from our model it is useful to translate the non-dimensional quantities back into physical parameters. Using the parameters λ_c, x_c, and α_c given in equation (3.2) we can derive the relations

$$I_c = \sqrt{\frac{2\alpha_c g\rho d}{\mu_0}}\ell, \tag{5.1}$$

$$L_c = \lambda_c \ell, \tag{5.2}$$

$$h_c = x_c \ell, \tag{5.3}$$

for the electric current I_c, and the initial (L_c) and instantaneous (h_c) height of fluid for which the current limiting effect will first occur. If we assume in addition that the system has a finite length L_y in the y-direction then the total electric resistance of the left-hand section $R = L_y/\sigma d\ell x$ ($\sigma =$ electrical conductivity) can be used to compute the voltage $U = RI$ and the dissipated electric power $P = RI^2$ at critical current as

$$U_c = \sqrt{\frac{2\alpha_c g\rho}{d\mu_0}}\frac{L_y}{\sigma x_c}, \tag{5.4}$$

$$P_c = \frac{2\alpha_c g\rho L_y \ell}{\sigma \mu_0 x_c}. \tag{5.5}$$

Let us select $d_0 = 1$ mm, $\ell_0 = 5$ mm, $L_{y0} = 50$ mm as reference values for the geometry parameters and consider a family of systems related to the reference system by a scaling parameter s, i.e. $d = sd_0$, $\ell = s\ell_0$, $L_y = sL_{y0}$. Table 1 shows critical parameters for $s = 1$ and $s = 5$ both for an H-trough filled with a Ga–In–Sn eutectic alloy ($\rho = 6363\,\mathrm{kg\,m^{-3}}$, $\sigma = 3.307 \times 10^6 \Omega^{-1}\,\mathrm{m^{-1}}$) and for a two-fluid system consisting of a liquid sodium and potassium alloy ($\rho = 855\,\mathrm{kg\,m^{-3}}$, $\sigma = 2.46 \times 10^6 \Omega^{-1}\,\mathrm{m^{-1}}$) covered by kerosene, which is insulating and only slightly lighter ($\rho = 850\,\mathrm{kg\,m^{-3}}$). For the two-fluid system in a closed loop, i.e. the columns connected at the top and completely filled, the effective density is just the density difference between the two fluids. This

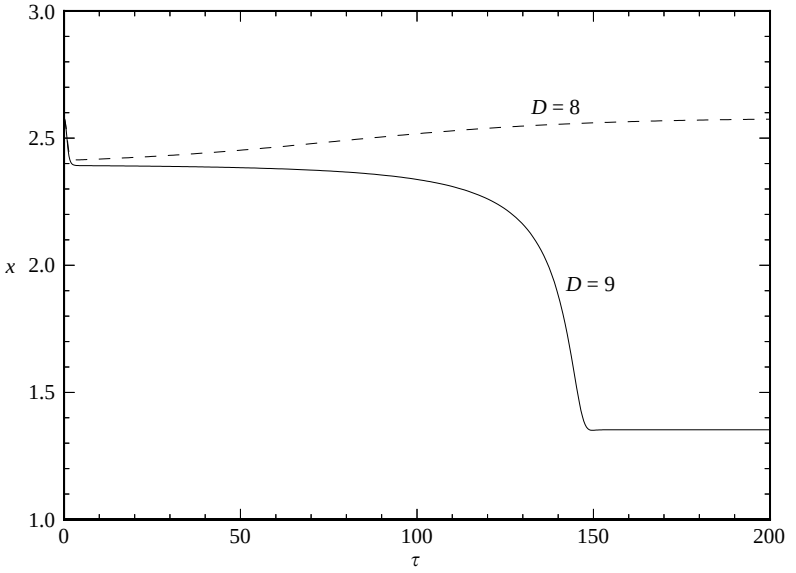

FIGURE 9. Response of the H-trough to a short current pulse given by (5.9).

leads to much lower critical currents, a fact which was exploited by Northrup (1907) in his experiments.

Furthermore, our expressions for the critical parameters permit one to understand how the performance characteristics of current limiters change with the size of the system. If we set $d = sd_0$, $\ell = s\ell_0$, and $L_y = sL_{y0}$ in (5.1), (5.4), and (5.5) we obtain the dependence of all parameters on the geometry scaling factor s in the form

$$I_c \sim s^{3/2}, \tag{5.6}$$

$$U_c \sim s^{1/2}, \tag{5.7}$$

$$P_c \sim s^2. \tag{5.8}$$

It follows that the critical current per unit mass $m \sim s^3$ scales as $I_c/m \sim s^{-3/2}$ implying that small devices are more efficient in current limitation than large ones. For practical applications the scaling behaviour at constant L_y, i.e. $d = sd_0$, $\ell = s\ell_0$, $L_y =$ const is equally important. It is readily verified that the pertinent scaling laws are $I_c \sim s^{3/2}$, $U_c \sim s^{-1/2}$, $P_c \sim s$, $m \sim s^2$, and $I_c/m \sim s^{-1/2}$. These scaling laws apply for the situation where the distance between the electrodes is kept constant.

Although we did not address the dynamical behaviour of our system in the present work, this is an issue of great practical importance. Figure 9 shows the response of the H-trough operating at its stationary solution $\alpha_0 = 46.618$, $x_0 = 2.5794$ to a short current pulse of the form

$$\alpha(\tau) = \alpha_0 + D[\Theta(\tau) - \Theta(\tau + 1)] \tag{5.9}$$

as obtained by numerically solving (2.17) with an additional linear friction term $\mu \mathrm{d}x/\mathrm{d}\tau$ on the left-hand side. After the current pulse with $D = 8$ the system returns to its stable state, whereas after a perturbation with $D = 9$ it switches to the current-limiting state. The friction coefficient in the numerical solution was (somewhat arbitrarily) chosen as $\mu = 2$ such that the system at $\alpha = 0$ is just at the boundary between damped oscillations ($\mu < 2$) and the aperiodic case ($\mu > 2$). For practical applications μ has to be estimated from laminar or turbulent friction laws for a

U-bend. Once this step has been performed, our simple theoretical model can be easily integrated into existing software for network simulations, and can be used to perform extensive parameter studies which would be impossible if one were to use the full three-dimensional equations of magnetohydrodynamics. In reality such a device would be part of an electrical network consisting of a voltage source and ohmic inductive impedances such as cables, motors, heaters etc. Then the current is dependent on the combined impedance of all devices and therefore will be limited by an strong increase of the device's resistance. However, modelling of this behaviour is beyond the scope of the present work.

Finally, we note that the three-dimensional instabilities, which prevented a continuation of the experimental curves in figure 8(*a*) to higher α, represent an interesting hydrodynamic phenomenon, closely related to the interface instabilities studied by Fautrelle & Sneyd (1998) as well as to pinch-off effects known from ordinary hydrodynamics (Eggers 1993, 1997). A natural first step towards the understanding of such instabilities would be to consider a single infinitely long vertical liquid-metal sheet carrying a prescribed electric current. For this system, which corresponds to a single left-hand column of the H-trough, it may be expected that the deformable surface $h(y, t)$ becomes unstable with respect to long waves beyond a critical electric current. Our observation from figure 8(*a*) that the three-dimensional instabilities occur for $\alpha \sim \lambda^2$ suggests that the critical current should scale with the fluid height as $I \sim L$, a fact that could be tested in an experiment. Further theoretical and experimental investigation of these effects could improve our understanding of the dynamics of the free surface under the influence of Lorentz forces.

We are grateful to E. Zienicke, Ch. Karcher, U. Lüdtke, R. Gerner and F. Berger for interesting discussions and to E. Roth and R. Klein for their help with the experiments. Y. K.'s visiting professorship at Ilmenau University of Technology was supported by the Deutscher Akademischer Austauschdienst and by a Gerhard-Mercator-Gastprofessur of the Deutsche Forschungsgemeinschaft. T. B. is supported by an Emmy Noether fellowship of the Deutsche Forschungsgemeinschaft (grant number Bo 1668/2-1). Part of the work was performed during T. B.'s stay at Ilmenau University of Technology with financial support from the Deutsche Forschungsgemeinschaft in the framework of the "Forschergruppe Magnetofluiddynamik". We finally wish to express our gratitude to three anonymous referees whose insightful comments helped us to improve the presentation of the material.

REFERENCES

Berger, F., Dühr, O., Krätzschmar, A. & Terhoeven, P. 2001 Physical effects and arc characteristics of liquid metal current limiters. *Proc. 9th Intl Conf. on Switching Arc Phenomena, SAP 2001, 17–20 September 2001, Lodz, Poland*, pp. 272–277. Politechnika Lodzka, ISBN 83-902688-9-2, Lodz, Poland.

Biskamp, D. 1993 *Nonlinear Magnetohydrodynamics*. Cambridge University Press.

Bojarevics, V., Freibergs, T., Shilova, E. V. & Shcherbinin, E. V. 1988 *Electrically Induced Vortical Flows*. Kluwer.

Davidson, P. A. 1999 Magnetohydrodynamics in materials processing. *Annu. Rev. Fluid Mech.* **31**, 273–300.

Davidson, P. A. 2001 *An Introduction to Magnetohydrodynamics*. Cambridge University Press.

Doedel, E. J. 1981 AUTO: a program for the automatic bifurcation analysis of autonomous systems. *Cong. Num.* **30**, 265–284.

Doedel, E. J., Champneys, A. R., Fairgrieve, T. F., Kuznetsov, Y. A., Sandstede, B. & Wang, X. 1988 *AUTO97: Continuation and Bifurcation Software for Ordinary Differential Equations.* Concordia University, Montreal.

Eggers, J. 1993 Universal pinching of three-dimensional axisymmetric free-surface flow. *Phys. Rev. Lett.* **71**, 3458–3460.

Eggers, J. 1997 Nonlinear dynamics and breakup of free-surface flows. *Rev. Mod. Phys.* **69**, 865–930.

Fautrelle, Y. & Sneyd, A. D. 1998 Instability of a plane conducting free surface submitted to an alternating magnetic field. *J. Fluid Mech.* **375**, 65–83.

Gerner, R. 2004 Theoretical investigations of an electric current limiter based on the H-trough model. MSc Thesis, Ilmenau University of Technology (in German).

Hunt, J. C. R. 1991 Industrial and environmental fluid mechanics. *Annu. Rev. Fluid Mech.* **23**, 1–41.

Mohring, J. U., Karcher, C. & Schulze, D. 2004 Dynamic behavior of a liquid metal interface under the influence of a high frequency magnetic field. *Phys. Rev.* E (in press).

Moreau, R. 1990 *Magnetohydrodynamics.* Kluwer.

Murty, G. S. 1960 Instability of conducting fluid cylinder due to axial current. *Arkiv för Fysik* **18**, 241–250.

Northrup, E. F. 1907 Some newly observed manifestations of forces in the interior of an electric conductor. *Phys. Rev.* **24**, 474–497.

Seydel, R. 1994 *Practical Bifurcation and Stability Analysis.* Springer.

Terhoeven, P., Berger, F., Krätzschmar, A. & Freyermuth, T. 2001 Selbsterholende Strombegrenzungseinrichtung mit Flüssigmetall. German Patent DE 001 0018564 A1.

Thess, A., Boeck, Th., Terhoeven, P., Krätzschmar, A. & Freyermuth, Th. 2002 Selbsterholende Strombegrenzungseinrichtung mit Flüssigmetall. German Patent DE 102 43 993 B3.